Short Communication

Response Surface Methodology and Performance Analyses of the Activated Carbon Electrode for Electrosorptive Deionization

Haojie Liu[1,*], Haihong Li[1], Ke Yang[2]

[1] College of Environmental and Chemical Engineering, Xi'an Polytechnic University, Xi'an 710048, China.
[2] Shaanxi Automobile Commercial vehicle, Baoji 722405, China.
[*]E-mail: ykkm0101m@163.com, 569698405@qq.com

When researching the preparation of electrosorption electrodes, many researchers usually activate the material; however, in this study, we directly activated the electrode. An electrosorption electrode made of activated carbon was directly activated by cyclic voltammetry, and the activation conditions were optimized based on the response surface methodology. An optimal model was obtained featuring a sulfuric acid solution concentration of 3.00 $mol \cdot L^{-1}$, a scan rate of 0.01 $V \cdot s^{-1}$, and a scan cycle of 12.38, and the model was verified to be reliable. The surface morphology of the electrode material before and after activation was observed by scanning electron microscopy. The results showed that the activated electrode material had abundant pores. The electrochemical properties of the electrosorption electrodes were tested by an electrochemical workstation. The results showed that the specific capacitance of the activated electrode reached 219.98 $F \cdot g^{-1}$, which is 127% higher than the capacitance before activation, and the impedance was reduced from 29.99 Ω to 9.7 Ω, and the charge/discharge performance at high current density was good. In addition, the results of the electrosorption deionization experiment indicated that the ion removal rate of the activated electrode was 51.85%, compared with 35.48% before activation, and the electrosorption capacity of the electrode after activation was significantly improved. This study provides a reference for the development of electrosorption technology.

1. INTRODUCTION

High-salinity wastewater not only contains high amounts of organic pollutants, but also contains a large amount of mineral salt, which can inhibit the activity of microorganisms in sewage treatment, corrode water treatment equipment, and cause soil salinization. Thus, treating high-salinity wastewater is a challenging process in the water treatment industry [1]. In recent years, capacitive deionization (CDI) technology has emerged as a high-salinity wastewater treatment technology because of its low cost, high

ion removal rate, lack of secondary pollution and good renewable performance [2]. As shown in Fig. 1, the function of CDI depends on electrosorption electrodes. When saline water flows through the positive and negative electrodes, the ions in the water will move toward electrodes driven by the electric field force and then be adsorbed and stored in a double electric layer to obtain fresh water. After the electrosorption reaches saturation, electrode regeneration can be completed by reversing the connection of the two electrodes and backflushing with a small amount of fresh water.
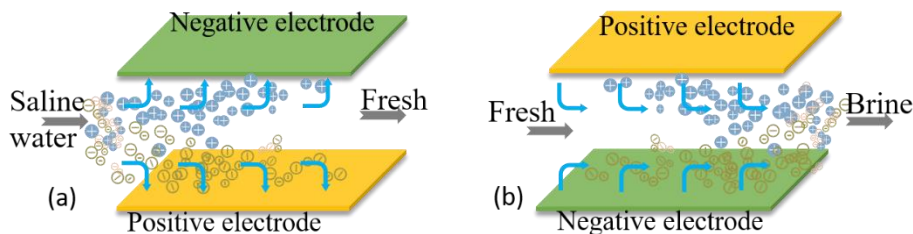
Figure 1. The principle of electrosorption (a) and desorption (b)

At present, research on electrosorption technology has mainly focused on electrode materials and current collectors [3, 4]. Researchers usually mix activated materials with a conductive agent and a binder in a certain proportion and then coat them onto a collector to make electrosorption electrodes [5-9]. Nevertheless, there are few studies on the direct and integral activation of electrodes and more studies on the activation or modification of raw materials. For instance, Wang et al. (2019) modified activated carbon with tetrabutyl titanate, and the specific capacitance of the obtained TiO_2-AC electrode was increased by 55.2% [7]. Wei et al. (2018) reported that electrodes made from sulfur-doped graphene aerogels showed a higher removal rate of lead ions than electrodes without sulfur [8].

Although the properties of these modified electrodes are improved, the addition of auxiliary reagents during preparation will still affect the electrode. We found that the direct electrochemical activation of an electrode can also enhance its performance, which is beneficial for improving the electrosorption capacity. This method avoids uncontrollable factors in the preparation process. A recent study showed that the electrochemical activation of an activated carbon electrode loaded with Ni-Co hydroxide results in more than 99% coulombic efficiency, which significantly improves the performance of the electrode [9]. Furthermore, different electrolyte conditions can greatly affect the performance of the electrode [10], and in the previous work, we found that when the electrode was activated by cyclic voltammetry, the scan rate and the scan cycle had a great impact on the electrode. Therefore, this study directly carried out electrochemical activation of an electrode based on response surface methodology to explore the interactive effects of electrolyte condition, scan rate, and scan cycle on the performance of the electrode. In addition, the micromorphology, electrochemical performance and deionization performance of the electrode before and after activation were analyzed, which provides a reference for the study of electroadsorption technology.

2. EXPERIMENTAL

2.1 Raw materials and chemicals

Activated carbon (AC, Tianjin North Fine Chemical Co., Ltd); polyvinylidene fluoride (PVDF, Taiyuan Yingze Liziyuan Battery Co., Ltd); dimethylacetamide (DMA, Tianjin Fuchen Chemical Reagent Factory); graphene nanoplatelets (GAN, Chengdu Aikeda Chemical Reagent Co., Ltd); 9 cm ×6 cm ×1 mm graphite collector; sulfuric acid (A. R, Sichuan Xilong Chemical Co., Ltd); sodium chloride (A. R, Tianjin Hedong District Hongyan Reagent Factory).

2.2 Preparation and activation

(1) First, 0.1 g of PVDF was added to a beaker, and then 10 ml of DMA was added as a solvent to completely dissolve PVDF under ultrasonic conditions. Then, 0.1 g of GAN and 0.8 g of AC were added and stirred well. At 80 °C constant temperature, the mixture was evenly coated onto the surface of the collector, and an electrosorption electrode was obtained after drying.

(2) With different concentrations of sulfuric acid as electrolytes and different scan cycles and scan rates (Table 1), electrodes were electrochemically activated by an electrochemical workstation. After activation was completed, the electrodes were rinsed with deionized water and then dried.

2.3 Experimental methods

Response surface methodology (RSM) is a combination of mathematics and statistics that models and analyzes problems in which the response value is affected by multiple variables and finally optimizes the response value [11]. Central composite design (CCD) is a kind of RSM. This method is considered effective at quickly screening out key factors from multivariable systems and optimizing experimental process conditions [12]. In this study, the factors and levels of the CCD experiment were designed by Design Expert software on the basis of a single-factor pre-experiment, as shown in Table 1. The purpose of this method is to obtain the optimal parameters for electrochemical activation and to mark the corresponding electrode as ETD-B. The unactivated electrode is marked as ETD-A.

Table 1. Factors and levels of the CCD experiment

Factor	Level		
	-1	0	1
A: Concentration/mol·L^{-1}	2.8	3	3.2
B: Scan rate/V·s^{-1}	0.008	0.01	0.012
C: Scan cycle	10	12	14

2.4 Characterization

The micromorphology of the active material on the electrode surface before and after activation was observed by scanning electron microscopy (SEM, Quanta-450-FEG, American FEI Company). The cyclic voltammetry, chronopotentiometry, and electrochemical impedance spectroscopy (EIS) of the electrode were tested by an electrochemical workstation (CHI610, Shanghai Chenhua Instrument Co., Ltd), and the specific capacitance value was calculated.

Calculation of specific capacitance: $C_S = \dfrac{1}{mv(U_f - U_i)} \int_{U_i}^{U_f} I(U)\,dU$ (1)

where Cs is the mass specific capacitance (F·g⁻¹), m is the mass of active materials (g), v is the scan rate (V·s⁻¹), U_i is the initial voltage (V), U_f is the final voltage (V), and $\int_{Ui}^{Uf} I(U)\,dU$ is the integral of the cyclic voltammetry curve calculated by Origin software.

3. RESULTS AND DISCUSSION

3.1 Analysis of the CCD experiment

3.1.1 Regression model and analysis of variance

The CCD experiment was designed by Design Expert software, and the experimental data are shown in Table 2. We fitted the data in the table and established a regression equation on the specific capacitance value, which is shown as Equation (2). At the same time, we also performed an analysis of variances on the data, as shown in Table 3.

$Y=219.63+3.19\times A-2.76\times B+5.22\times C+12.98\times A\times B+10.61\times A\times C+21.02\times B\times C-12.17\times A^2-19.29\times B^2-18.68\times C^2$ (2)

where Y is the specific capacitance, A is the concentration, B is the scan rate, C is the scan cycle.

Table 2. Data from the CCD experiment

Number	A/mol·L⁻¹	B/V·s⁻¹	C	Y/F·g⁻¹
1	3.00	0.01	12	223.05
2	3.00	0.01	12	218.36
3	3.00	0.01	15.36	157.77
4	2.80	0.012	14	181.64
5	3.20	0.012	10	136.51
6	3.00	0.01	12	219.59
7	3.00	0.013	12	144.59
8	2.66	0.01	12	159.72
9	3.00	0.007	12	177.33
10	2.80	0.008	10	202.52

11	3.00	0.01	12	215.36
12	3.00	0.01	12	222.59
13	3.20	0.012	14	231.51
14	3.20	0.008	10	158.05
15	3.00	0.01	12	220.24
16	2.80	0.012	10	148.64
17	3.00	0.01	8.64	167.56
18	3.20	0.008	14	149.4
19	3.34	0.01	12	202.47
20	2.80	0.008	14	170.99

Table 3. Variances of CCD experimental data

Variation	Sum of square	Degree of freedom	Mean square	F-value	P-value
Model	1697.77	9	1885.75	7.91	0.0017
A	139.05	1	139.05	0.58	0.4628
B	104.19	1	104.19	0.44	0.5236
C	372.82	1	372.82	1.56	0.2397
AB	1346.81	1	1346.81	5.65	0.0389
AC	900.58	1	900.58	3.78	0.0807
BC	3535.56	1	3535.56	14.82	0.0032
A^2	2133.38	1	2133.38	8.94	0.0136
B^2	5360.15	1	5360.15	22.47	0.0008
C^2	5030.31	1	5030.31	21.09	0.0010
Residual	2385.27	10	238.63		

The fitting degree of the regression model is evaluated by the goodness-of-fit test (R^2 test), and the closer R^2 is to 1, the higher the model fit. The R^2 of the specific capacitance value in this experiment is 87.66%. According to Table 3, the P-value of the regression model is 0.0017 (<0.05), which indicates that the correlation between the dependent variable and the independent variables is good, and the regression model has a high significance; that is, within the experimental value range, the fitting degree of the regression model is high [13-14]. In addition, the P-values of AB and BC are less than 0.05, indicating that there is an interaction between concentration and scan rate (AB) as well as scan rate and scan cycle (BC).

3.1.2 Response surface

The response surface can intuitively reflect the interaction of two variables on the specific capacitance value, as shown in Fig. 2, Fig. 3 and Fig. 4.
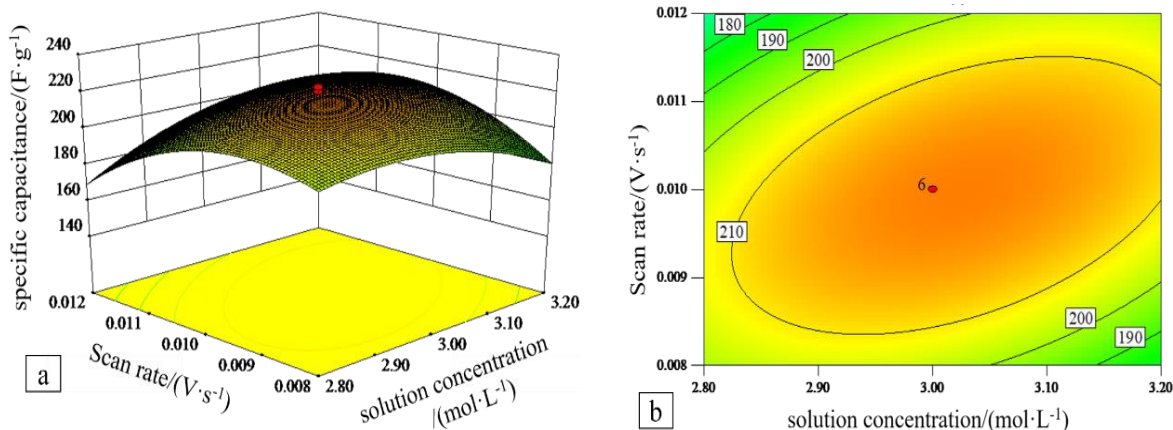
Figure 2. Interactive effect of sulfuric acid solution concentration and scan rate on specific capacitance: (a) response surface image of this effect, (b) isoline image of this effect.
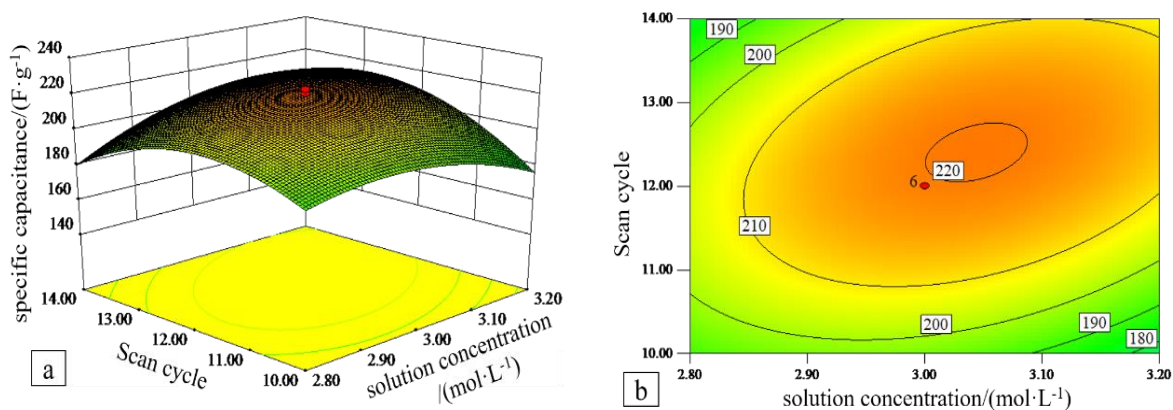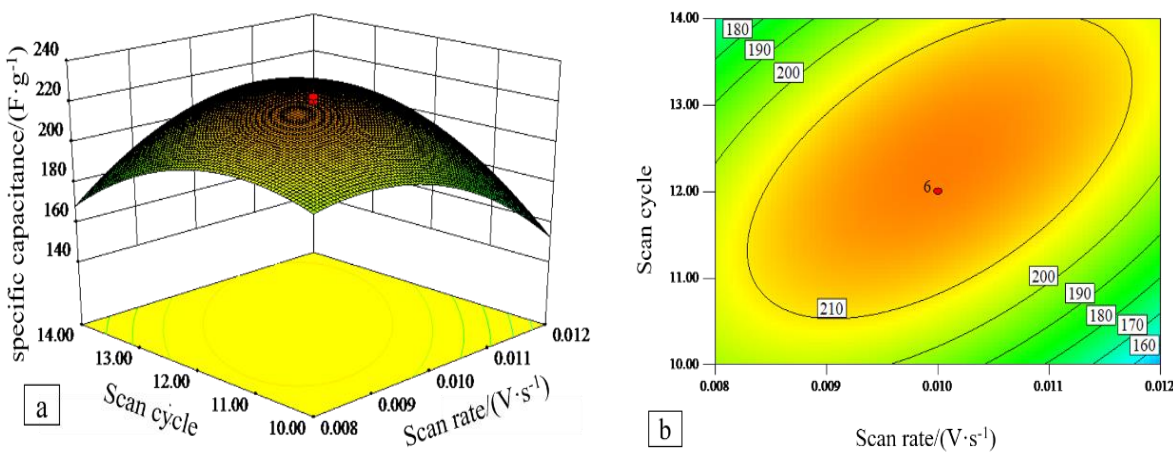

Figure 3. Interactive effect of sulfuric acid solution concentration and scan cycle on specific capacitance: (a) response surface image of this effect, (b) isoline image of this effect.

Figure 4. Interactive effect of scan cycle and scan rate on specific capacitance: (a) response surface image of this effect, (b) isoline image of this effect.

According to these response surfaces (Fig. 2a, Fig. 3a, Fig. 4a), within the value range of each factor, by keeping one of them unchanged, the specific capacitance value will first increase first and then decrease as the other factor increases. Therefore, each response surface appears as a convex surface with maximum points. The convex shape in Fig. 4a is more obvious, indicating that the interaction of scan rate and scan cycle is more significant, which is consistent with the analysis in the previous section. This is because when the concentration of the electrolyte is low, the electrode is not fully activated [15-16]. As the concentration increases, the electrode is fully activated, and its specific capacitance increases. However, when the concentration is too high, the pores inside the materials are corroded, resulting in a reduced specific capacitance (Fig. 2a, Fig. 3a). In addition, when the scan rate is slower, the electron transfer is slower, and the specific capacitance of the electrode is lower, but if the scan rate is too fast, the electrons have no residence time [17-19], so the specific capacitance is also reduced (Fig. 2a, Fig. 4a). In addition, if the scan cycle is too low, electrons cannot reach the components of the materials, resulting in a smaller specific capacitance, but if the scan cycle is too high, there are no extra sites on the electrode for electrons to occupy; then, later electrons will attract the original electrons and fall off [20], thus reducing the specific capacitance (Fig. 3a, Fig. 4a). Fig. 2b shows that when the concentration is approximately 3.00 mol·L^{-1} and the scan rate is approximately 0.01 V·s^{-1}, the specific capacitance value reaches the extreme point. Fig. 3b shows that when the concentration is approximately 3.00 mol·L^{-1} and the scan cycle is approximately 12, the specific capacitance value reaches the extreme point. Fig. 4b shows that when the scan rate is approximately 0.01 V·s^{-1} and the scan cycle is approximately 12, the specific capacitance value reaches the extreme point.

3.1.3 Model validation

The regression model was solved to obtain the predicted value: the concentration was 3.00 mol·L^{-1}, the scan rate was 0.01 V·s^{-1}, and the scan cycle was 12.38. Under these conditions, the response value of the specific capacitance reaches a maximum of 219.978 F·g^{-1}. To verify the reliability of the results, three sets of parallel experiments were performed under above the conditions, and the average value of the specific capacitance was calculated to be 218.98 F·g^{-1}. Compared with the predicted value, the error is only 0.45% (<10%), which indicates that the model is reliable. Therefore, this model can be used as the optimal activation condition for the electrosorption electrodes. In recent reports, Liu et al. [21] prepared chemically modified activated carbon onto an electrode with a specific capacitance of 123.8 F·g^{-1}, and Cuong et al. [22] prepared rice husk biochar onto an activated carbon electrode with a specific capacitance of 120.5 F·g^{-1}; compared with these studies, the electrode we prepared has a higher specific capacitance.

3.2 Micromorphology

The surface morphologies of the unactivated electrode (ETD-A) and the activated electrode (ETD-B) were observed by SEM, as shown in Fig. 5.
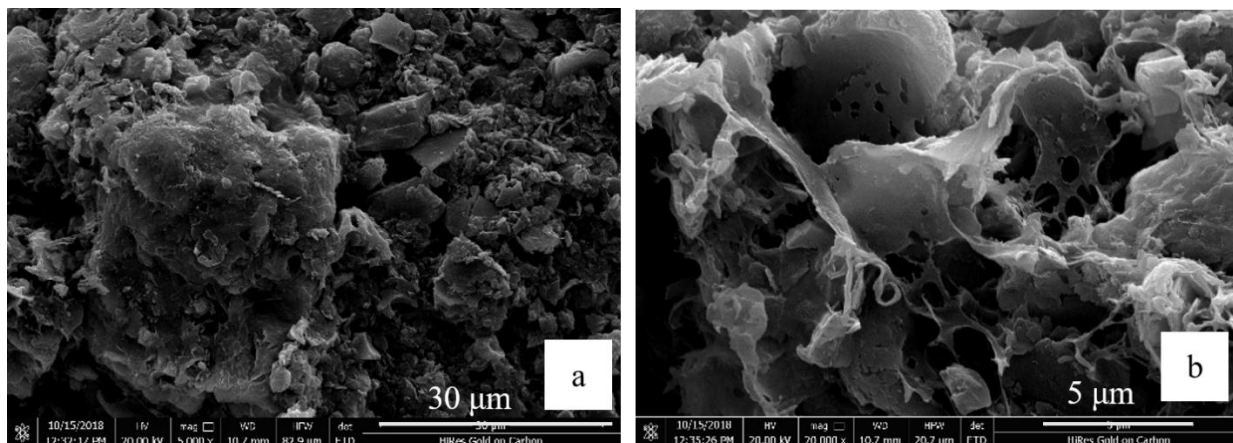
Figure 5. SEM images: (a) the unactivated electrode (ETD-A) and (b) the electrode obtained under optimal activation conditions (ETD-B).

It can be seen from Fig. 5a that the active materials on the surface of the ETD-A electrode before activation are granular aggregates. After electrochemical activation, the pores of the active materials are opened, and the surface shows honeycomb-shaped grooves and holes, as shown in Fig. 5b. This indicates that electrochemical activation changes the structure of activated carbon to create more developed pores, which increases the contact area between liquid and active materials and indirectly enhances the electrode's electrosorption capacity. Ma et al. [23] increased the pore size of activated carbon by chemical modification, which is conducive to ion migration and improves the efficiency of electrosorption and desorption. Yin et al. [24] optimized the pore structures of electrode materials, which improved the ion removal rate by 60%.

3.3 Analysis of cyclic voltammetry

Cyclic voltammetry tests were performed on the ETD-A electrode and ETD-B electrode, and CV curves are shown in Fig. 6.
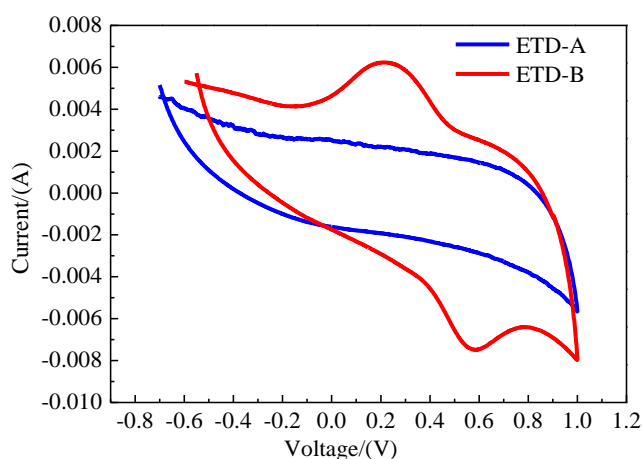

Figure 6. CV curves of ETD-A and ETD-B measured at a scan rate of $0.05 \ V \cdot s^{-1}$ in $0.5 \ mol \cdot L^{-1}$ NaCl aqueous solution.

Theoretically, the CV curve is a symmetric rectangle, but in an actual system, the CV curve often exhibits deviation due to the polarized internal resistance of the electrode [25-26]. According to Fig. 6, in a voltage range of -0.7 V to 1.0 V, both curves have symmetry, but the closed curve area of the ETD-B electrode is larger than that of ETD-A. It can be seen from formula (1) that the larger the area of the CV curve is, the larger the specific capacitance, that is, the larger the electrosorption capacity. Using formula (1), the specific capacitance of ETD-A is 96.57 F·g⁻¹, the specific capacitance of ETD-B is 219.98 F·g⁻¹, and the specific capacitance is increased by 127% after activation. In addition, redox peaks appear on the CV curve of ETD-B, indicating that the electrode has not only electric double-layer capacitance but also Faraday capacitance. The potential difference between the oxidation peak and the reduction peak of the CV curve of ETD-B is only 0.367 V. The smaller the potential difference is, the higher the reversibility of the electrode [27-28], which means that the electrosorption-desorption performance is improved.

3.4 Chronopotentiometry

In a voltage range of 0.05 V~0.8 V, the charge/discharge performance of the ETD-B electrode was measured by chronopotentiometry (CP) at different current densities, as shown in Fig. 7.
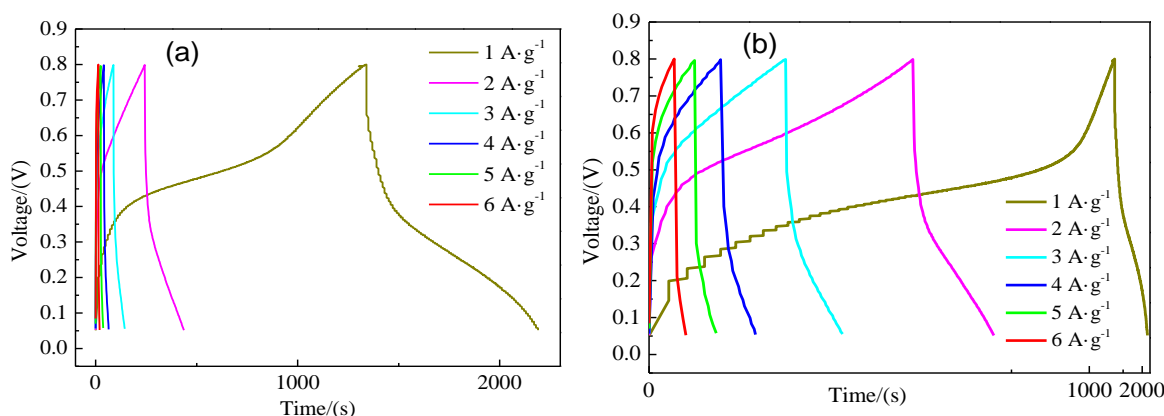

Figure 7. CP curve of the ETD-B electrode: b is the transverse magnification of a; voltage range from 0.05 V to 0.08 V; current density from 1 A·g⁻¹ to 6 A·g⁻¹.

After calculation, the corresponding specific capacitance values of the ETD-B electrode are 114.05 F·g⁻¹, 114.16 F·g⁻¹, 115.46 F·g⁻¹, 118.96 F·g⁻¹, 121.85 F·g⁻¹, and 125.19 F·g⁻¹ at current densities of 1 A·g⁻¹, 2 A·g⁻¹, 3 A·g⁻¹, 4 A·g⁻¹, 5 A·g⁻¹, and 6 A·g⁻¹. The specific capacitance of the ETD-B electrode increases with increasing current density. In addition, as shown in Fig. 7, as the current density increases, the charge/discharge period of the electrode decreases, and at the same time, the CP curve approaches an isosceles triangle, which indicates that the performance of the electrosorption-desorption is better at high current density [29-31].

3.5 Analysis of EIS

EIS curves of ETD-A and ETD-B electrodes are shown in Fig. 8.

According to Fig. 8, in the middle- and high-frequency regions, an arc appears in both curves, and the projected width of the arc reflects the charge transfer resistance. The smaller the charge transfer resistance is, the faster the electron transfer rate [32-33]. Compared to the ETD-A electrode (Fig. 8a), the charge transfer resistance of the ETD-B electrode (Fig. 8b) is significantly reduced, from approximately 15.4 Ω to 3.3 Ω, indicating that the rate of ion adsorption on the ETD-B electrode is faster. The value of the intersection between the arc and the real axis is the contact resistance. As shown in Fig. 8, the contact resistance of the ETD-B electrode is significantly lower than that of the ETD-A electrode. In the low-frequency region, theoretically, there will be a section of the Warburg straight line with a tilt of 45° [34]. In Fig 8, both electrodes show a straight line of approximately 45°, which indicates that the electrochemical performance is good, but the ion diffusion process of the electrode materials is affected to some extent [35].
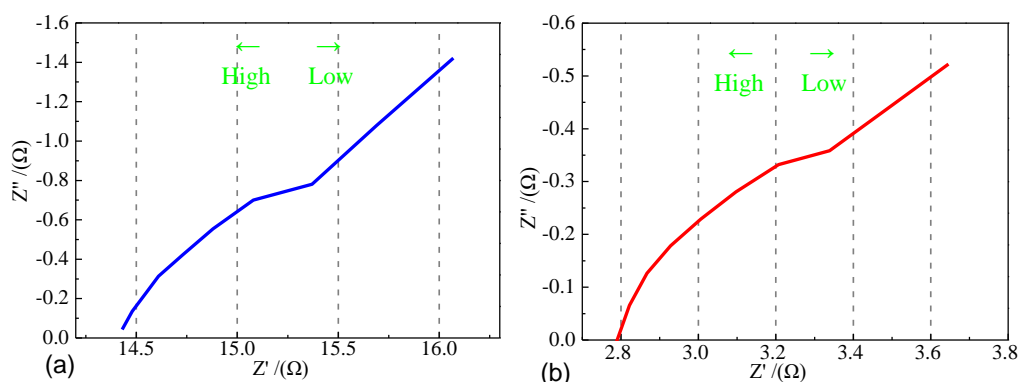

Figure 8. EIS curves of the ETD-A electrode (a) and ETD-B electrode (b): measured in 0.5 mol·L^{-1} NaCl aqueous solution; frequency range from 0.001 kHz to 100 kHz with 5 mV amplitude.

Fig. 9 shows the equivalent circuit diagram obtained by fitting EIS data with Z-View software, and the impedance values of each equivalent component are shown in Table 4.
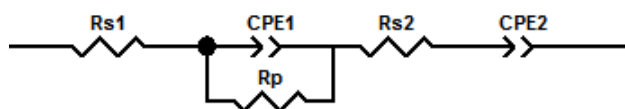

Figure 9. Equivalent circuit

Table 4. Impedance values of components in the equivalent circuit

Sample	R_{S1}/Ω	R_{S2}/Ω	C_{PE1}/Ω	C_{PE2}/Ω	R_P/Ω	Total impedance/Ω
ETD-A	14.38	14.54	0.660	0.526	3.191	29.99
ETD-B	4.667	4.363	0.83	0.28	0.732	9.70

According to Table 4, after activation, the impedance value of the ETD-B electrode decreases obviously, indicating that under the optimal model, the electrode obtained by activation has a lower impedance, which is beneficial to the electrosorption process.

3.6 Electrosorption experiment

The ETD-A electrode and ETD-B electrode were used for an electrosorption experiment to treat an NaCl solution with a concentration of 25000 mg·L^{-1}. The change in electrical conductivity as the indicator reflects the change in concentration is shown in Fig. 10.
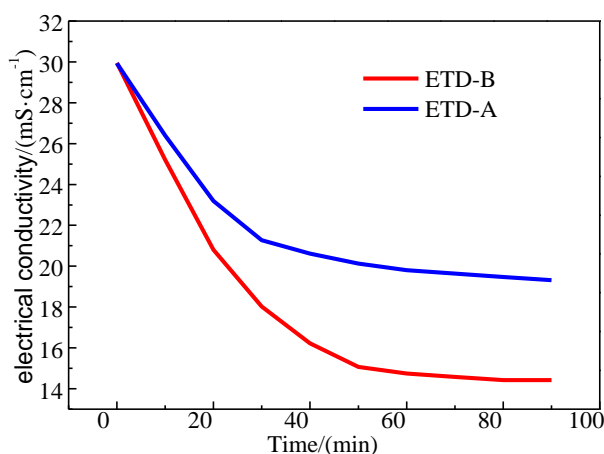

Figure 10. Electrosorption of ETD-A and ETD-B: initial conductivity is 29.95 mS·cm^{-1}, and after ETD-A and ETD-B treatment, the electrical conductivity of the solution was 19.31 mS·cm^{-1} and 14.41 mS·cm^{-1}, respectively. Voltage 1.2 V; electrode spacing 10 mm.

It can be seen from Fig. 10 that both electrodes gradually reach electrosorption saturation after 60 min, and the conductivity change rate of the solution processed by the ETD-B electrode is always fast, indicating that the ETD-B electrode has a faster electrosorption rate. In addition, the decrease in the conductivity of the solution treated by the ETD-B electrode is significantly larger. The ion removal rates of the ETD-A electrode and ETD-B electrode are 35.48% and 51.85%, respectively, indicating that the ETD-B electrode has a larger electrosorption capacity. In summary, electrochemical activation of the electrosorption electrode can effectively increase its electrosorption capacity.

4. CONCLUSIONS

In summary, we successfully electrochemically activated an activated carbon electrode based on RSM and analyzed the performance of the electrosorption electrode obtained under the optimal model. The results are as follows:

(1) A regression model of the specific capacitance was established by CCD experiments. The optimal activation conditions obtained for the model solution included a sulfuric acid solution concentration of 3.00 mol·L^{-1}, a scan rate of 0.01 V·s^{-1}, and a scan cycle of 12.38. Under these conditions, the predicted value of the specific capacitance is 219.978 F·g^{-1}. The actual value is 218.98 F·g^{-1}, and the error is only 0.45% (<10%) compared to the predicted value, which proves that the model is reliable.

(2) The active materials on the surface of the activated ETD-B electrode are no longer aggregated and have more holes. The specific capacitance of the ETD-B electrode reaches 219.98 F·g^{-1}, which is 127% higher than the capacitance of the unactivated electrode. The charge/discharge performance of the ETD-B electrode at high current density is good. In addition, the total impedances of the ETD-B electrode and ETD-A electrode are 9.7 Ω and 29.99 Ω, respectively, indicating that the activation significantly reduces the impedance.

(3) In an electrosorption experiment, the ion removal rates of the ETD-A electrode and ETD-B electrode are 35.48% and 51.85%, respectively, which proves that the work effectively improved the electrosorption performance of the electrode.

References

1. X. Li, M.M. Gou, X.F. Liu, R.T. Baiya, *Technology of Water Treatment*, 45 (2019) 6-10+14.
2. Y.C. WU, D.W. Ying, Y.L. Wang, J.P. Jia, *Technology of Water Treatment*, 45 (2019) 1-6+15.
3. C.C. Tang, R.M. Xu, *Modern Chemical Industry*, 39 (2019) 15-19+23.
4. Y. Lester, E. Shaulsky, R. Epsztein, I. Zucker, *Separation and Purification Technology*, 237(2020) 116388.
5. H.H. Li, J. Yang, C. Zhang, H.Y. Li, P.P. Pei, *Journal of Porous Materials,* 22 (2015) 887-895.
6. Z. Wang, L Wang, L. Ma, J.T. Fu, *Applied Chemical Industry,* 48 (2019) 775-779.
7. J. Wang, H.H. Li, K. Hou, Q. Zhang, *Fresenius Environment Bulletin,* 28 (2019) 5877-5887.
8. Y. Wei, W. Zhao, W.H. Yao,X.D. Jiang, Q.Q. Ma, *Environmental Chemistry,* 37 (2018) 2305-2314.
9. X.C. Shao, In-situ activation and electromical properties of 3D Ni-Co-based nanoarrays electrode, *Guangxi University*, China, (2018).
10. W. Qian, F. Sun, Y. Xu, *Energy & Environmental Science,* 7 (2014) 379-386.
11. Y.F. Wang, C.G. Wang, *Journal of Minzu University of China (Natural Sciences Edition)*, 3 (2005) 236-240.
12. S. Qiu, Study of two classes of composite designs, *Central China Normal University,* China, (2018).
13. Z.Q. Zhang, Q. Zhou, M.X. Wu, *Journal of Yangtze University(Natural Science Edition),* 10 (2019) 67-71.
14. Y. Zheng, M.C. *Chen, Industrial Water Treatment,* 6 (2019) 43-47.
15. S. Pan, L.D. Tang, B. Wang, J.G. Qi, L. Liu, *Electronic Components and Materials,* 12 (2019) 14-20+27.
16. W.G. Zhu, Q. Lv, J.X. Lu, G.X. Zuo, F. Jiang, *Journal of Mudanjiang Normal University (Natural*

Sciences Edition), 2 (2019) 21-24.
17. D.X. Zhang, J.Y. Xue, *Applied Chemical Industry,* 6 (2016) 1187-1190.
18. T. Zhang, W.K. Zhang, *Journal of Synthetic Crystals,* 12 (2019) 2265-2269.
19. P. Wang, Y. Feng, M. Sun, *Electronic Components and Materials,* 8 (2019) 13-19.
20. Y. Li, D.H. Wang, G.J. Zhao, W.L. Wu, H. Zhu, *Journal of Wuhan University (Natural Science Edition),* 3 (2015) 213-218.
21. X.Y. Liu, Y.N. Wang, X.J. Lu, C. Chen, X.H. Wu, J. Mao, *Industrial Water Treatment,* 2 (2020) 23-27.
22. D.V. Cuong, P.C. Wu, N.L. Liu, C.H. Hou, *Separation and Purification Technology*, 242 (2020) 116813.
23. L. Ma, L. Wang, Z.H. Xia, Z. Wang, J.T. Fu, *Applied Chemical Industry,* 4 (2018) 716-720+729.
24. J. Yin, F. Cheng, R.X. Su, J.L. Zhang, *Technology of Water Treatment,* 7 (2018) 49-53.
25. Y.N. Li, C. Tan, J.S. Li, Z. Xia, J.L. Zuo, *Journal of Harbin University of Commerce (Natural Sciences Edition),* 35 (2019) 657-661.
26. Q. Qin, Y.J. Chen, S.M. Xie, C.S. Nong, J.H. Hu, M. Li, *Industrial Water Treatment,* 39 (2019) 25-28.
27. Ö. Çelebican, I. İnci, N. Baylan, *Journal of Molecular Structure*, 1203 (2020) 127312.
28. L.M. Chang, X.Y. Duan, W. Liu, *Desalination*, 270 (2011) 285-290.
29. Y. Wang, H.H. Li, J. Wang, *Journal of Functional Materials,* 1 (2020) 1109-1114.
30. W.G. Su, C. Zhang, Y.H. Bai, X.D. Song, G.S. Yu, *Acta Petrolei Sinica (Petroleum Processing Section),* 1 (2020) 78-85.
31. A. Raja, P. Rajasekaran, K. Selvakumar, M. Arunpandian, S.A. Bahadur, M. Swaminathan, *Electrochimica Acta,* 328 (2019) 135062.
32. M.W. Li, S.Z. Liu, Y.G. Wang, S.B. Yang, *Journal of the Chinese Ceramic Society,* 9 (2019) 1320-1326.
33. F.P. Wang, J. Ma, K.L. Zhou, X.Y. Li, *Materials Chemistry and Physics,* 244 (2020) 122215.
34. S.C. Yang, G.X. Pan, M.H. Xu, K. Zhou, X.T. Liu, Y.Z. Shen, *Chemical Research and Application,* 1 (2020) 72-78.
35. J.F. Shi, M.X. Sun, *Modern Chemical Industry,* 6 (2019) 162-165.
36. J.H. Choi, *Separation and Purification Technology,* 70 (2010) 362-366.
37. S.Y. Liu, R.C. Wang, C.X. Ma, X.Y Zhou, D.H. Yang, *China Environmental Science*, 39 (2019) 3866-3871.
38. S.Y. Li, X. Chen, *Journal of Henan Normal University (Natural Science Edition)*, 47 (2019) 76-81.
39. H.D. Wu, Q.D. Qiao, Z.X. Yang, J.Q. Shao, *New Chemical Materials*, 46 (2018) 180-182+186.
40. Y. Yang, C. Zhang, *China Measurement & Test*, 44 (2018) 35-41.